Water adsorption and dissociation on BeO (001) and (100) surfaces

Maria A. Gomez [a]

[a] *Department of Chemistry, Mount Holyoke College, 50 College Street, South Hadley, MA 01075*

Lawrence R. Pratt and Joel D. Kress [b]

[b] *Theoretical Division, Los Alamos National Laboratory, Los Alamos, NM 87545*

D. Asthagiri [c]

[c] *Department of Chemical and Biomolecular Engineering, John Hopkins University, 3400 North Charles Street, Baltimore, MD 21218*

Surface Science, in press 2007

Abstract

Plateaus in water adsorption isotherms on hydroxylated BeO surfaces suggest significant differences between the hydroxylated (100) and (001) surface structures and reactivities. Density functional theory structures and energies clarify these differences. Using relaxed surface energies, a Wulff construction yields a prism crystal shape exposing long (100) sides and much smaller (001) faces. This is consistent with the BeO prisms observed when beryllium metal is oxidized. A water oxygen atom binds to a single surface beryllium ion in the preferred adsorption geometry on either surface. The water oxygen/beryllium bonding is stronger on the surface with greater beryllium atom exposure, namely the less-stable (001) surface. Water/beryllium coordination facilitates water dissociation. On the (001) surface, the dissociation products are a hydroxide bridging two beryllium ions and a metal coordinated hydride with some surface charge depletion. On the (100) surface, water dissociates into a hydroxide ligating a Be atom and a proton coordinated to a surface oxygen but the lowest energy water state on the (100) surface is the undissociated metal-coordinated water. The (100) fully hydroxylated surface structure has a hydrogen bonding network which facilitates rapid proton shuffling within the network. The corresponding (001) hydroxylated surface is fairly open and lacks internal hydrogen bonding. This supports previous experimental interpretations of the step in water adsorption isotherms. Further, when the (100) surface is heated to 1000 K, hydroxides and protons associate and water desorbs. The more open (001)

hydroxylated surface is stable at 1000 K. This is consistent with the experimental disappearance of the isotherm step when heating to 973 K.

---

1 Introduction

As a result of its low density, high melting point, nuclear properties, and stability, beryllium is used in aerospace, ceramics, electronics, nuclear energy and defense, metal recycling industries, dentistry, and even sporting goods [1]. Up to temperatures of 1534 K and pressures of 12 GPa, beryllium crystal is hexagonal closed packed (HCP) [2,3]. In air, beryllium oxide (BeO) forms on surfaces of beryllium metal[4,5]. BeO has been identified as an important component of beryllium aerosol exposures that lead to chronic beryllium disease (CBD), an incurable disease primarily of the pulmonary region of the lung[6]. Beryllium machining is likely to produce beryllium aerosol particles coated with BeO. Aerosol particles deposited in the pulmonary region of the lung are found in phagolysosomes within macrophage cells. In the low pH (about 4.8) of these macrophage vacuoles beryllium particles have been observed to undergo dissolution[7]. Studies in rats suggest that beryllium oxide can cause internal damage to macrophages which then aggregate and form granulomas [8]. Animal studies [9,10,11] as well as dissolution experiments [12,13] suggest that BeO calcined at 773 K (low fired) dissolves faster and leads to greater granuloma formation than BeO calcined at 1273K (high fired). More soluble beryllium compounds such as beryllium sulfate led to increased toxicity [14]. Understanding the solubilities of different beryllium compounds is important in determining risk factors for CBD as well as understanding the pathway from inhalation to the disease. Sutton and Burastero have studied how beryllium speciation and solubility is influenced by pH, beryllium concentration, and the composition of the dissolving fluid[15]. Since the mechanism of dissolution depends on the surface structure, characterizing common BeO surfaces and their reactivity is a useful first step. In the present study, we characterize the typical surfaces observed when BeO is formed by oxidizing beryllium metal and their hydroxylation. Hydroxylation can occur upon exposure to water vapor in air [16,17] prior to inhalation or at the latest when the BeO comes into contact with water in neutral pH lung tissue prior to ingestion by a macrophage. In a later study, we will consider the effect of the acidic environment within the phagolysosomes of the macrophage cell on BeO dissolution.

Beryllium oxide (BeO) is a Wurtzite crystal up to pressures of 137 GPa [18]. LEED experiments suggest that a six to seven monolayer BeO (001) film grows on top of Be(001). A new $p(2 \times 2)$ LEED pattern appears which suggests a surface reconstruction [19]. Crystal growth experiments on both Be/BeO and the analogous Zn/ZnO system suggest that when the metal is burned, needles

of the oxide appear. These needles grow into prisms. The top face of the prisms is the (001) face while the side of the prisms is the (100) face. Water adsorption studies on BeO crystals at temperatures below 973K show a plateau in the adsorption isotherms. This plateau is linked to fast water chemisorption on defect sites, followed by fast water adsorption on the hydroxylated (001) and $(00\bar{1})$ surfaces, followed by a slow water adsorption on the hydroxylated (100) surface. Hydroxylation of the (001) and $(00\bar{1})$ surfaces was expected to yield fairly isolated hydroxyl groups which could readily hydrogen bond to adsorbed water [16,17]. In contrast, hydroxylation of the (100) surface was expected to yield a network of hydrogen bonded hydroxyls which would attract additional water molecules for comparatively weak absorption.

The plateau in the adsorption isotherms becomes less pronounced as the temperature rises until it is completely gone by 973K. IR spectra of the same systems show a decrease in hydroxylation with increasing temperature until there is no OH stretch signal at 973K and beyond. It is suggested that surface rumpling at higher temperatures occludes the beryllium and disrupts the hydrogen-bond network among surface hydroxyls [16,17]. The temperature range below which hydrogen-bonded surface-hydroxyl network forms (973 K) is in between the high and low fired calcined BeO temperatures [9]. Basic chemistry suggests that the hydroxylation structure of the different BeO surfaces plays an important role in how the surfaces interact with water and hence the dissolution process. The calcined BeO and animal studies suggest that solubility is important to the formation of granulomas and development of CBD [12,13,14].

This paper compares density functional theory geometries and energies for water adsorption, dissociation, and the resulting hydroxylation on the (001) and (100) BeO surfaces. These surfaces are exposed when BeO grows on Be(001). Understanding hydroxylation of these surfaces is a prerequisite to understand the dissolution. Section 2 describes the method used to calculate bulk BeO lattice parameters. Section 3 presents the (001), $(00\bar{1})$ and (100) BeO surface cuts and relaxations. Water adsorption and dissociation on these surfaces is discussed in section 4. Section 5 describes the hydroxylated surface structures. Finally, in section 6, our findings are discussed in relation to available experiments.

2 Bulk

The Vienna Ab-initio Simulation Package (VASP [20,21,22,23]) implementation of density functional theory with the generalized gradient approximation and the RPBE functional [24] was used for all calculations. The projector augmented wave (PAW) potentials were used as supplied by Kresse and Hafner

[25,26]. Specifically, the valence states of Be:$1s^2 2s^2$ and O: $2s^2 2p^4$ were used. The actual occupancies are adjusted during the self-consistent field electronic cycles while maintaining the total number of electrons fixed. K-point meshes were generated using the $\Gamma-$point shift. The cutoff for the plane waves was 400 eV. Electronic optimization stops when the total system energy and the band structure energy of successive steps differs by less than 10^{-5} eV. Projection operators were evaluated in reciprocal space. Electronic optimization used the the special Davidson block iteration scheme implemented in VASP[27,28]. Gaussian smearing with a width of 0.1 eV was used. Geometry optimizations used a conjugate gradient method. The geometry optimization stops when successive energy differences are less than 10^{-4} eV. Ions, cell shape and cell volume were varied. Precision was kept at the accurate level to avoid wrap around errors for a very accurate bulk calculation. Bulk calculations used a primitive mesh of $8 \times 8 \times 6$ k-points. The Wurtzite primitive vectors $(\sqrt{3}a/2, -a/2, 0)$, $(0, a, 0)$, and $(0, 0, c)$ were used in the optimizations. This corresponds to a slab of dimensions $a \times a \times c$. The a and c lattice constants found were 2.71 and 4.39 Å, respectively. These values compare well with experimental values of 2.6967(1) and 4.3778(1) Å[29].

3 (001), (00$\bar{1}$) and (100) BeO surface relaxations

The total cell size (slab and vacuum) and shape are kept at their bulk values while relaxing the surfaces. Additionally, the inner two BeO layers are kept at the bulk geometry. The conditions for electronic and nuclear optimization are the same as for the bulk unless otherwise noted.

As shown in Figure 1 (a), a cut through the (001) plane results in a non-symmetric slab with a (001) surface on one end and the (00$\bar{1}$) surface at the other end. This gives rise to a dipole which induces a reconstruction when the surface is six to seven layers thick [19]. As can be seen from Table 1, a six layer slab of area $a \times a$ with vacuum-width of 14.76 Å is sufficient to converge surface energies. Throughout this paper, the width of the vacuum layer is defined as the distance between the outermost atoms in the simulation box surfaces along the z and x directions for (001)/(00$\bar{1}$) and (100) surfaces, respectively. An adatom is never considered as an outermost surface atom. The (001)/(00$\bar{1}$) calculations use a k-point mesh of $8 \times 8 \times 1$ and dipole corrections.

Fowler, *et al.*, [19] postulated a reconstruction of a (001)/(00$\bar{1}$) slab where 1/4 of either cation vacancies or adsorbed anions form on the (001) surface and the same number of adsorbed cations or anion vacancies form on the (00$\bar{1}$) side. The LEED pattern is consistent with the anion and cation additions appearing in their normal lattice sites. The six layer $a \times a$ slabs used for the surface relaxations only contain single beryllium and oxygen ions on each

surface. Therefore, moving 1/4 of the cations or anions from one surface to another requires a surface that is at least $2a \times 2a$. Comparing the relaxed structures of this minimum size surface and a $4a \times 4a$ surface revealed that the minimum size was not large enough. Using a $2 \times 2 \times 1$ k-point grid on a six layer $3a \times 3a$ slab with a 19.15 Å wide vacuum layer yielded a relaxed surface energy of 0.203 eV/Å^2 which is in agreement with the relaxation energy of the smaller surfaces with a larger grid. This suggested that a $2 \times 2 \times 1$ k-point grid is sufficient for these larger surfaces. Optimizations were started from: (i) a relaxed surface slab with 1/4 of the cations moved from the (001) side to the $(00\bar{1})$ side and (ii) a relaxed surface slab with 1/4 of the anions from the $(00\bar{1})$ side moved to the (001) side. The lowest energy minimum in both cases shifts the displaced ions from their normal lattice sites to binding in three fold sites. As seen in Table 1, the $p(2\times2)_i$ and $p(2\times2)_{ii}$ reconstructed surfaces have lower surface energies than the unreconstructed $(001)/(00\bar{1})$ surfaces. The lowest energy reconstructed surface found is shown in Figure 1 (b). The exposed (001) surface of this structure is consistent with the LEED pattern. However, there is discrepancy on the unexposed $(00\bar{1})$ surface. In the experiment, ions are kept in lattice positions by the beryllium metal below. Since our system does not have a BeO/Be interface the beryllium atoms are displaced from their normal lattice positions to three-fold sites on the $(00\bar{1})$ surface.

Table 1 also shows the surface energies of different (100) slabs using k-point grid of $1 \times 8 \times 6$. A three layer $a \times c$ slab with 9.87 Å of vacuum is sufficient for converging (100) surface energies. The dipole correction was negligible for this surface. Figure 2 displays our relaxed (100) surface. The distortions from bulk show the same trends as the previous calculations of Jaffe and Zapol[30]. For example, the distance between surface beryllium and oxygen atoms in the relaxed surface structure is 1.50 Å in our calculations and 1.48 Å in their calculation. The same distance for atoms just below the surface is 1.67 Å in our calculation and 1.63 Å in their calculation. In both calculations, oxygens occlude beryllium.

4 Water adsorption and dissociation

A water molecule was placed on each surface in a geometry intended to favor bonding. After optimization of the initial structures, neighboring geometries were sampled using molecular dynamics (MD) on the Born-Oppenheimer surface with a time step of 1 fs and temperature re-scaling of velocities every 10 steps at 800 K. No equilibration was done. This is a sampling scheme similar to forced bias[31], smart[32], and hybrid[33] Monte Carlo schemes rather than a true dynamics. The Γ point and a 300 eV plane wave cut off was used in this low precision sampling process. Water dissociation occurred within 500 MD steps on the (001) surface. On the (100), after many trials a dissociation was

observed within 2000 MD steps. The geometries sampled were visualized and a low-energy subset was chosen for subsequent conjugate gradient optimization. The final optimizations used the earlier 600 eV plane wave cutoff and default precision. (001)/(00$\bar{1}$) and (100) adsorbate optimizations used $2 \times 2 \times 1$ and $1 \times 2 \times 2$ k-point meshes, respectively.

These optimizations revealed adsorbed and dissociated water configurations. Water adsorbs on the (100) surface both with a water oxygen bonded directly to a surface beryllium ion *and* with a hydrogen bond to a surface oxygen atom. After several trials starting from a bound water, water molecule dissociation was seen in a high-temperature trajectory. Other times, the water molecule desorbed. On the (001) surface which exposes beryllium, only surface Be-OH_2 bonds were observed. Water dissociated readily on the unreconstructed (001) surface.

When a trajectory produced water molecule dissociation, the Nudged Elastic Band (NEB)[34] method was used to find the transition pathway. Six linearly interpolated images between adsorbed and dissociated water were used. When NEB suggested intermediate minima, the minima were refined and a new shorter path NEB calculation was done. Once NEB was converged, climbing NEB [35] was implemented to refine the transition state. Table 2 shows the system size and binding energies of water in the adsorbed, transition state, and dissociated forms on (001) and (100) surfaces. All these energies are relative to the corresponding bare relaxed surface plus an isolated water molecule. The dissociated product on the (001) surface is 2.57 eV lower in energy than the undissociated bound water. The dissociation barrier is only 0.12 eV. In contrast, the dissociation barrier on the (100) surface is 0.57 eV and the dissociated product is 0.36 eV higher in energy than the undissociated bound water. This explains why water dissociates more readily on the (001) surface than on the (100) surface. The size of the (001) surface needed for reconstruction made water dissociation studies on it computationally prohibitive.

Figure 3 shows the corresponding water adsorption and dissociated geometries on the (001) surface. The transition state looks similar to the bound water minimum and hence is not shown. Figure 4 shows the water adsorption, transition state, and dissociated geometries found for the (100) surface. Water dissociation on the (001) surface differed significantly from dissociation on (100). On the (001) surface Be-OH_2 loses a hydrogen to a nearby beryllium atom. The hydroxide shifts to coordinate with a second beryllium. Bader analysis [36] of the electron charge density suggests that a hydride and a hydroxide have been formed, as the hydrogen and hydroxide charges are -0.71 and -1.06, respectively. To compensate, there is a lower electron density among some of the other surface atoms. When more waters are added, further hydroxylation is possible. *In this case, dynamic runs show hydrogen atoms combining, leaving as hydrogen gas, thus giving a direct demonstration of partial oxidation of the*

beryllium. In contrast, on the (100) surface, water dissociates into a hydroxide coordinated to a single surface beryllium and a proton which binds to a surface oxygen. Bader charge density analysis of the dissociated water on the (100) surface reveals a -1.01 charge on the hydroxide and a $+1.00$ charge on the proton. As can be seen in Figure 4, the dissociated configuration permits hydrogen bonding between the hydroxide oxygen and the adjacent proton.

5 Hydroxylated surface structure

Surfaces were fully hydroxylated as suggested by the dissociation patterns seen in the molecular dynamics sampling. The hydroxylated surfaces were optimized using the Γ point. From this configuration, a sampling molecular dynamics was started. Configurations from this run were then optimized. There are in principle many orientations possible for all the hydroxide combinations and this is by no means an exhaustive minima search. Nevertheless, Figures 5 (a) and (b) show a representative hydroxylation structure for the (001) and (100) surfaces, respectively. The (001) surface tended to form doubly-coordinated metal hydroxide structures, and to lose hydrogen gas leading to a sparsely hydroxylated (001) surface. Additionally, once some doubly-coordinated beryllium ions are produced, the chance for further hydroxylation decreases. Hence, the surface hydroxylation was not homogeneous as seen in the sample configuration shown in Figure 5 (a). All the nonbonded oxygen/hydrogen distances there are larger than 3 Å, *i.e.*, longer than traditional hydrogen bonds.

In contrast, the tendency of the (100) surface to dissociate water molecules into a hydroxide and proton on adjacent surface beryllium and oxygen ions leads to a denser hydroxylation. On this hydroxylated surface, adjacent nonbonded oxygens and hydrogens have distances in the range of 1.6 to 1.9 Å. In addition, sometimes a row of adjacent hydroxides and protons associated to beryllium bonded water, and occasionally more than one row associated in that way. This is consistent with the hydrogen bonded network postulated in references [16,17] to explain the step in water adsorption data.

Heating the (100) hydroxylated surface to 1000 K lead to proton shuffling and association of hydroxide ligands with protons followed by water desorption of several water molecules. The same heating of the (001) hydroxylated surface left the hydroxylated structure unchanged.

6 Concluding discussion

Bulk lattice parameters agree with experiment[29]. Beryllium oxide prisms with prominent (100) sides and smaller (001) tops grow on Be(001) [16,17] in the laboratory. Consistent with this, a Wulff construction [37,38] based on the surface energies in Table 1 suggests that BeO crystals exposing (100), (001) and $(00\bar{1})$ faces exhibit a prism shape with large (100) faces and small (001) and $(00\bar{1})$ faces. Some synthetic crystals which expose these faces have the same prism shape [39]. When BeO is grown on Be(001), the BeO$(00\bar{1})$ face is hidden by the Be(001). There are also alternative ways to make BeO crystals which expose additional phases and exhibit different crystal patterns [40,41].

In agreement with LEED experiments [19] where thin layers of BeO are grown on Be(001), a p(2x2) lower energy reconstruction of the BeO(001) is found. Nevertheless, our lowest energy reconstruction has beryllium in three fold sites rather than at the standard lattice positions. This is likely a result of not having a Be(001) substrate attached to the BeO$(00\bar{1})$ surface in our simulations. The (001) surface reconstruction is consistent with the experiment.

Water adsorption and dissociation reveals a reactive unreconstructed (001) surface consistent with preferred BeO growth in the direction of the (001) surface normal making more (100) surface. The preferred state of water on the (001) surface is in the dissociated form. In contrast, on the (100) surface, water prefers to physi-sorb. The size of the (001) reconstructed simulation cells prohibited detailed study of water/surface reactivity on these systems. Since the reconstructed flatter (001) surface has beryllium only slightly higher than oxygens, water surface reactivity is expected to decrease relative to the unreconstructed surface. However, water reactivity should still be greater than for the (100) surface where surface berylliums are below surface oxygens.

Extensive hydroxylation of the unreconstructed (001) surface does not allow for much internal hydrogen bond formation. In contrast, hydroxylation of the (100) surface lends itself to a hydrogen bonded network. This might lead to a slower water adsorption until a new water layer capable of hydrogen bonding to additional water is added. This may explain the step in the adsorption isotherms. Finally, the hydrogen bonded network in the hydroxylated (100) surface allows for significant proton shuffling aiding association of hydroxide and proton into water. Desorption follows heating to 1000 K. This is consistent with the disappearance of the adsorption step and IR OH stretch signal following exposure to this temperature [16,17]. Nevertheless, in our simulations, the surface does not appear to have a permanent change.

The presence of reactive surfaces such as the (001) here might explain the high initial rates observed in dissolution studies[42], although dissolution of

BeO in aqueous media is acid catalyzed [43]. Therefore in sufficiently acidic solutions equilibration of surface structures should probably be expected after an initial rate. Then a hydroxylated surface may be an obligatory intermediate for the molecular mechanism of dissolution. Surface dehydroxylation at high temperatures might be indicative of annealing that could explain the slower dissolution of high fired beryllium oxide compared to low fired beryllium oxide.

7 Acknowledgments

We would like to thank Aleksandr B. Stefaniak and Ronald C. Scripsick for useful discussions. This work was carried out under the auspices of the National Nuclear Security Administration of the U.S. Department of Energy at Los Alamos National Laboratory under Contract No. DE-AC52-06NA25396.

References

[1] A. J. Stonehouse. Physics and chemistry of beryllium. *J. Vac. Sci. Technol. A*, 4(3):1163–1173, 1986.

[2] V. Vijayakumer, B. K. Godwal, Y. K. Vohra, S. K. Sikka, and R. Chidambaram. On the high-pressure phase transition in beryllium metal. *J. Phys. F: Met. Phys.*, 14:L65–L68, 1984.

[3] L. C. Ming and M. H. Manghnani. Isothermal compression and phase transition in beryllium to 28.3 gpa. *J. Phys. F: Met. Phys.*, 14:L1–L8, 1984.

[4] R. O. Adams and J. T Hurd. The properties of beryllium surfaces and films. *J. Less-Common Metals*, 18:399–409, 1969.

[5] M. D Hoover, B. T. Castorina, G. L. Finch, and S. J. Rothenberg. Determination of the oxide layer thickness on beryllium metal particles. *Am. Ind. Hyg. Assoc. J.*, 50:550–553, 1989.

[6] A. B. Stefaniak, M. D. Hoover, G. A. Day, R. M. Dickerson, E. J. Peterson, M. S. Kent, C. R. Schuler, P. N. Breysse, and R. C. Scripsick. Characterization of physicochemical properties of beryllium aerosols associated with prevalence of chronic beryllium disease. *J. Environ. Monit.*, 6:1–11, 2004.

[7] S. Sturgill-Koszycki, P. H. Schlesinger, P. Chakraborty, P. L. Haddix, H. L. Collins, A. K. Fok, R. D. Allen, S. L. Gluck, J. Heuser, and D. G. Russel. Lack of acidification in mycobacterium phagosomes produced by exclusion of the vesicular proton-atpase. *Science*, 263:678–681, 1994.

[8] C. L. Sanders, W. C. Cannon, G. J. Powers, R. R Adee, and D. M. Meier. Toxicology of high-fired beryllium oxide inchaled by rodents. *Arch. Env. Health*, 30:546–551, 1975.

[9] P. J. Haley, D. E. Bice, B. A. Muggenburg, M. D. Hoover, F. F. Hahn, A. G. Harmsen, J. A. Mewhinney, and G. L. Finch. A canine model of beryllium-induced granulomatous lung disease. *Laboratory Investigation*, 61:219–227, 1989.

[10] P. J. Haley, K. F. Pavia, D. S. Swafford, D. R. Davila, M. D. Hoover, and G. L. Finch. The comparative pulmonary toxicity of beryllium metal and beryllium oxide in cynomolgus monkeys. *Immunopharmacology and Immunotoxicology*, 16(4):627–644, 1994.

[11] G. L. Finch, F. F. Hahn, and M. D. Hoover. Animal models of beryllium-induced lung disease. *Environmental Health Perspectives*, 104:973–975, 1989.

[12] A. B. Stefaniak, G. A. Day, M. D. Hoover, P. N. Breysse, and R. C. Scripsick. Differences in dissolution behavior in phagolysosomal simulant fluid for single-constituent and multi-constituent materials associated with beryllium sensitization and chronic beryllium disease. *Toxicology in Vitro*, 20:82–95, 2006.

[13] G. A. Day, M. D. Hoover, A. B. Stefaniak, R. M. Dikerson, E. J. Peterson, M. A. Esmen, and R. C. Scripsick. Bioavailability of beryllium oxide particles: An in vitro study in the murine j774a.1 macrophage cell line model. *Exp. Lung Res.*, 31:341–360, 2005.

[14] G. L. Finch, R. J. Verburg, J. A. Mewhinney, A. F. Eidson, and M. D. Hoover. The effect of beryllium compound solubility on in vitro canine alveolar macrophage cytotoxicity. *Toxicology Letts.*, 41:97–105, 1988.

[15] M. Sutton and S. R. Burastero. Beryllium chemical speciation in elemental human biological fluids. *Chem. Res. Toxicol.*, 16:1145–1154, 2003.

[16] T. Morimoto and M. Nagao. Adsorption anomaly in the system zinc oxide-water. *J. Phys. Chem*, 78(11):1116–1120, 1974.

[17] T. Miyazaki, y. Kuroda, K. Morishige, S. Kittaka, J. Umemura, T. Takenaka, and T. Morimoto. Interaction of the surface of BeO with water: In connection with the two-dimensional condensation of water. *J. Coll. Interf. Sci.*, 106(1):154–160, 1985.

[18] K. J. Chang and M. L. Cohen. Theoretical study of BeO. *Solid State Comm.*, 50(6):487–491, 1984.

[19] D. E. Fowler and J. M. Blakely. Surface reconstruction of BeO(0001) during be oxidation. *Surf. Sci.*, 148:283–291, 1984.

[20] G Kresse. *Thesis, Technische Universitat at Wien*, 1993.

[21] G Kresse and J Hafner. *Ab initio* molecular dynamics for liquid metals. *Phys. Rev. B*, 47:558–561, 1993.

[22] G Kresse and J. Furthmuller. Efficiency of *ab-initio* total energy calculations for metals and semiconductors. *Comput. Mater. Sci.*, 6:15–50, 1996.

[23] G Kresse and J. Furthmuller. Efficient iterative schemes for *ab initio* total-energy calculations using a plane-wave basis set method. *Phys. Rev. B*, 54:11169–11186, 1996.

[24] Yingkai Zhang and Weitao Yang. Comment on ıgeneralized gradient approximation made simplej. *Phys. Rev. Lett.*, 80(4):890, Jan 1998.

[25] P. E. Blochl. Projector augmented-wave method. *Phys. Rev. B*, 50:17953, 1994.

[26] G Kresse and J. Joubert. From ultrasoft pseudopotentials to the projector augmented wave method. *Phys. Rev. B*, 59:1758, 1999.

[27] E. R. Davidson. Methods in computational molecular physics. In G. H. F. Diercksen and S Wilson, editors, *NATO Advanced Study Institute, Series C*, volume 113, page 95, New York, 1983. Plenum.

[28] C. Moler and I. Shavitt, editors. *Report on Workshop "Numerical Algorithms in Chemistry: Algebraic Methods"*. Lawrence Berkeley Laboratories, University of California, 1978.

[29] O. Reckeweg, C. Lind, A. Simon, and F. J. DiSalvo. Rietveld refinement of the crystal structure of α-Be_3N_2 and the experimental determination of optical band gaps for Mg_3N_2, Ca_3N_2 and $CaMg_2N_2$. *Zeitschrift fur Naturforschung Section B-A J. Chemical Sciences*, 58(2-3):159 – 162, 2003.

[30] J. E. Jaffe and P. Zapol. Atomic relaxation of the BeO (1010) surface. *Surf. Sci.*, 381:L563–567, 1997.

[31] C Pangali, M. Rao, and B. J. Berne. Novel monte-carlo scheme for simulating water and aqueous-solutions. *Chemical Physics Letters*, 55(3):413–417, 1978.

[32] P. J. Rossky, J. D. Doll, and H. L. Friedman. Brownian dynamics as smart monte-carlo simulation. *Journal of Chemical Physics*, 69(10):4628–4633, 1978.

[33] S. Duane, A. D. Kennedy, B. J. Pendleton, and Roweth D. Hybrid monte-carlo. *Physics Letters B*, 195(2):216–222, 1987.

[34] G. Henkelman and H. Jonsson. Improved tangent estimate in the nudged elastic band method for finding minimum energy paths and saddle points. *J. Chem. Phys.*, 113:9978, 2000.

[35] G. Henkelman, B. P. Uberuaga, and H. Jonsson. A climbing image nudged elastic band method for finding saddle points and minimum energy paths. *J. Chem. Phys.*, 113:9901, 2000.

[36] G. Henkelman, A. Arnaldsson, and H. Jonsson. A fast and robust algorithm for bader decomposition of charge density. *Comput. Mater. Sci.*, in press, 2005.

[37] M. Abramowski, R. W. Grimes, and S. Owens. Morphology of UO_2. *J. Nuc. Mat.*, 275:12–18, 1999.

[38] G Wulff. Zur frage der geschwindigkeit des wachstums und der auflosung der kristallflachen. *Z. Kristallogr.*, 34:449–530, 1901.

[39] B. Austerman. Growth of beryllia single crystals. *J. Am. Cer. Soc.*, 46:6–10, 1963.

[40] B. Austerman. Growth and properties of beryllium oxide single crystals. *J. Nuc. Mat.*, 14:225–236, 1964.

[41] B. Austerman. Flux process for growth of large cyrstals with application to beryllia. *J. Crystal Growth*, 42:284–288, 1977.

[42] G. L. Finch, J. A. Mewhinney, A. F. Edison, M. D. Hoover, and S. J. Rothenberg. In vitro dissolution characteristics of beryllium oxide and beryllium metal aerosols. *J. Aerosol Sci.*, 19:333–342, 1989.

[43] G. Furrer and W. Stumm. The coordination chemistry of weathering: I. dissolution kinetics of δ-Al_2O_3 and BeO. *Geochim. Cosmochim. Acta*, 50:1847–1860, 1986.

List of Tables

List of Figures

3 Water can dissociate on the (001) surface by first binding to a beryllium on the surface (a), stretching an OH bond in the direction of a beryllium, and finally reaching a dissociated state (b). The transition state looks similar to (a) and hence is not shown. This dissociated state involves a hydroxyl, a hydride, and some electron density reductions on the surface. The white spheres are hydrogens. Multiple paths to this type of dissociation are possible. This is a representative one. 19

4 Water can dissociate on the (100) surface by first binding to a beryllium on the surface (a), going through a transition state in which the water hydrogen bonds to an adjacent oxygen (b), and finally reaching a dissociated state (c). This dissociated state involves a proton and a hydroxide. 20

5 (a) Hydroxylated (001) surface viewed from the $< 001 >$ direction. (b) Hydroxylated (100) viewed from the $< 100 >$ direction. 21

Table 1
Surface energies per unit surface area. Vacuum length is defined by the distance from the outermost atom on one surface to the outermost atom on the other surface along the z or x axes for the (001)/(00$\bar{1}$), denoted (001), and (100) surfaces, respectively. An adatom is never considered as an outermost surface atom. $p(2\times 2)_i$ and $p(2\times 2)_{ii}$ are the reconstructions moving: (i) 1/4 cations moved from the (001) side to the (00$\bar{1}$) side and (ii) 1/4 anions from the (00$\bar{1}$) side moved to the (001) side. See Section 3 for more details. See Figures 1 (a) and 2 for pictures of the relaxed but unreconstructed (001) and (100) surfaces. Figure 1(b) shows the $p(2\times 2)_i$ reconstructed structure.

Surface	Slab Dimensions		Vacuum	Surface Energy (eV/Å^2)	
	Area	Layers	Height (Å)	Unrelaxed	Relaxed
Unreconstructed (001):	$a\times a$	6	14.76	0.220	0.194
	$a\times a$	6	19.15	0.218	0.193
	$a\times a$	8	19.10	0.221	0.198
$p(2\times 2)_i$	$4a\times 4a$	6	19.39		0.090
$p(2\times 2)_{ii}$	$4a\times 4a$	6	18.96		0.113
(100) :	$a\times c$	3	9.87	0.120	0.069
	$a\times c$	4	12.58	0.120	0.070

Table 2
The system size and binding energies of water in the adsorbed, transition state, and dissociated forms on (001) and (100) surfaces. All these energies are relative to the corresponding bare relaxed surface plus an isolated water molecule. The corresponding structures are shown in Figures 3 and 4, respectively. Moving the hydride in the (001) structure lowers the energy further.

Surface	Slab Dimensions		Vacuum	Binding Energy (eV)		
	Area	Layers	Height (Å)	Adsorption	Transition State	Dissociation
(001):	$3a \times 3a$	6	19.15	-1.28	-1.16	-3.85
(100):	$3a \times 2c$	3	26.12	-0.75	-0.18	-0.39

Fig. 1. (a) A 001 cut reveals two surfaces: The top (001) surface viewed from the side features exposed Be atoms while the bottom $(00\bar{1})$ surface buries them. The $(00\bar{1})$ surface is adjacent to the Be(001) face when the beryllium oxidizes. (b) As can be seen from a top view of the reconstructed (001) surface, this lowest energy reconstructed surface has Be atom vacancies (black circles) in the flattened (001) face and additional Be atoms at three fold sites (light grey spheres in the center of hexagons) on the $(00\bar{1})$ face. In all figures, the small light grey and large dark grey spheres are Be and O, respectively.

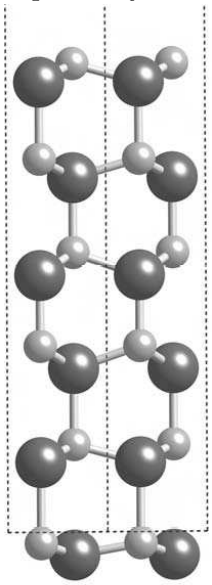

(a)

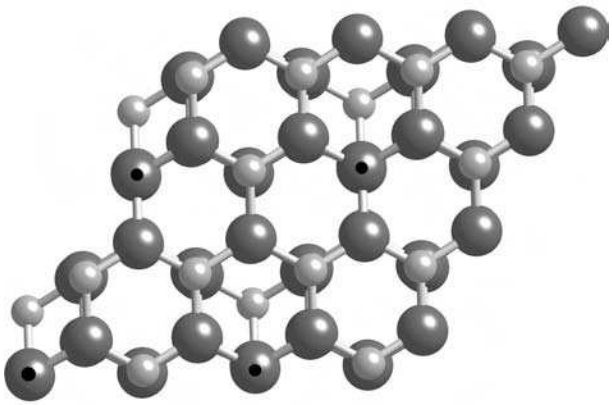

(b)

Fig. 2. The (100) cut reveals two symmetric (100) surfaces. In this relaxed surface, the surface beryllium ions are slightly lower than the oxygens.

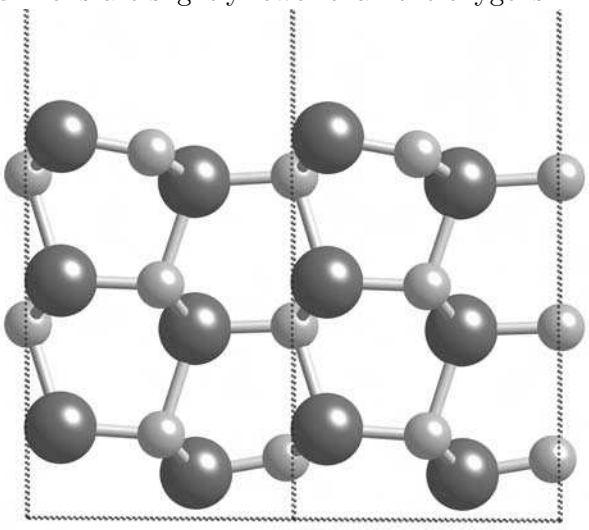

Fig. 3. Water can dissociate on the (001) surface by first binding to a beryllium on the surface (a), stretching an OH bond in the direction of a beryllium, and finally reaching a dissociated state (b). The transition state looks similar to (a) and hence is not shown. This dissociated state involves a hydroxyl, a hydride, and some electron density reductions on the surface. The white spheres are hydrogens. Multiple paths to this type of dissociation are possible. This is a representative one.

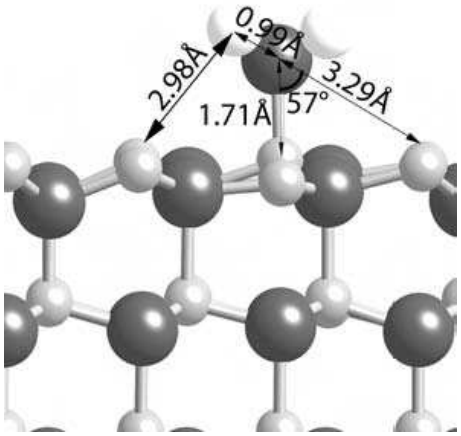

(a)

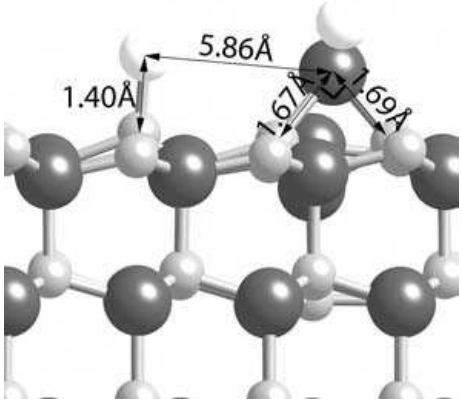

(b)

Fig. 4. Water can dissociate on the (100) surface by first binding to a beryllium on the surface (a), going through a transition state in which the water hydrogen bonds to an adjacent oxygen (b), and finally reaching a dissociated state (c). This dissociated state involves a proton and a hydroxide.

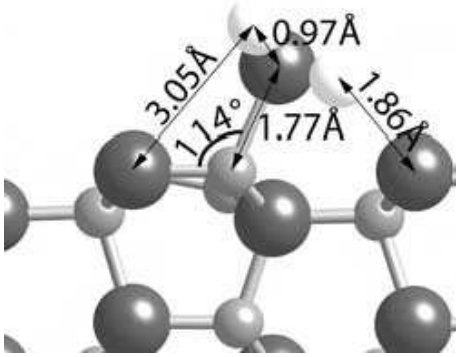

(a)

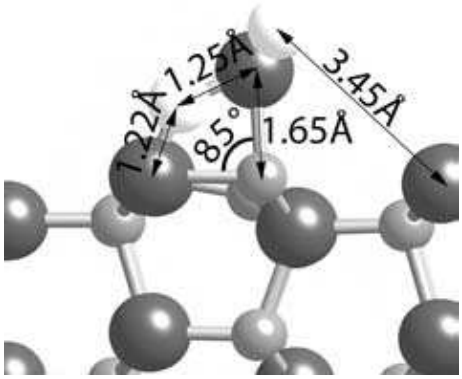

(b)

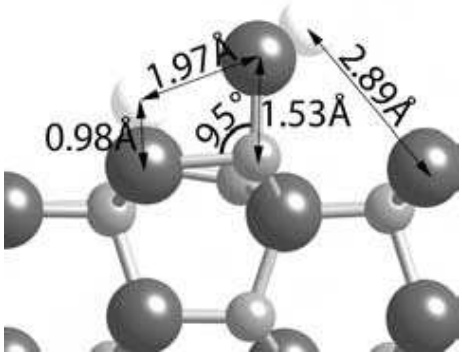

(c)

Fig. 5. (a) Hydroxylated (001) surface viewed from the $< 001 >$ direction. (b) Hydroxylated (100) viewed from the $< 100 >$ direction.

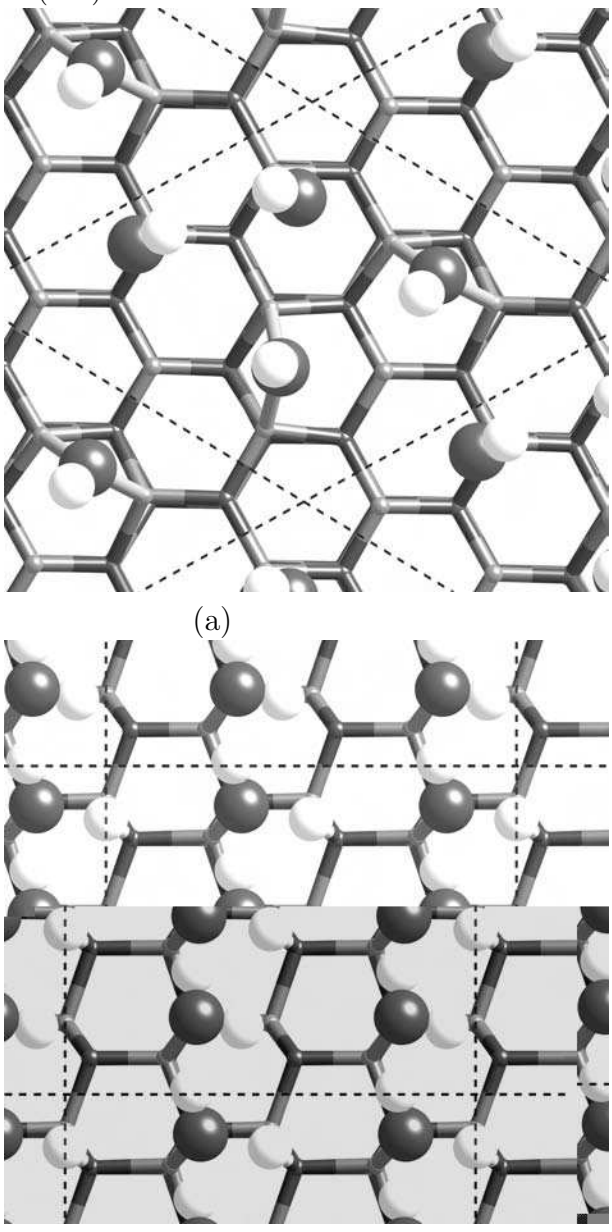

(a)

(b)